Numerical investigation of the impact of geological discontinuities on the propagation of ground vibrations

Ali Haghnejad[1a], Kaveh Ahangari[*1], Parviz Moarefvand[2] and Kamran Goshtasbi[3]

[1]*Department of Mining Engineering, Science and Research Branch, Islamic Azad University, Tehran, Iran*
[2]*Department of Mining and Metallurgical Engineering, Amirkabir University of Technology, Tehran, Iran*
[3]*Department of Mining Engineering, Tarbiat Modares University, Tehran, Iran*

Abstract. Blast-induced ground vibrations by a significant amount of explosives may cause many problems for mining slope stability. Geological discontinuities have a significant influence on the transmission of dynamic pressure of detonation and according to their position relative to the slope face may have damaging or useful impacts on the slope stability. In this study, the effect of geological discontinuities was investigated by modelling a slope with geological discontinuities through applying the dynamic pressure in three-dimensional discrete element code (3DEC). The geological discontinuities in four states that generally apperceived in mine slopes are considered. Given the advantages of the pressure decay function defined by some researcher, this type of function was used to develop the pressure-time profile. The peak particle velocities (PPV) values were monitored along an axis by utilization of Fish programming language and the results were used as an indicator to measure the effects. As shown in the discontinuity-free model, PPV empirical models are reliable in rocks lacking discontinuities or tightly jointed rock masses. According to the other results, the empirical models cannot be used for the case where the rock mass contains discontinuities with any direction or dip. With regard to PPVs, when the direction of discontinuities is opposite to that of the slope face, the dynamic pressure of detonation is significantly damped toward the slope direction at the surface of discontinuities. On the other hand, when the discontinuities are horizontal, the dynamic pressure of detonation affects the rock mass to a large distance.

Keywords: geological discontinuities; detonation pressure; PPV; slope stability; 3DEC

1. Introduction

Due to adaptability, drilling and blasting are the most economical and viable methods of extracting rock masses in different geological conditions (Yang *et al.* 2016). During rock blasting, a huge amount of energy is released of explosives in the form of tension (up to 50 GPa) and temperature (up to 5000 K). According to literature, up to 30% of energy is consumed for breakage and the rest is consumed for ground vibration, back breaking, air blasting, etc. Due to the reduction of rock mass strength, ground vibration is of extreme importance in terms of slope stability. Given the high volume extraction in large open pit mines, a large amount of explosives is used in each blasting operation. This volume of explosives produces a high dynamic pressure, which may have adverse effects on the slope stability due to possible ground vibration (Azizabadi *et al.* 2014, Aksoy *et al.* 2016). The impact of ground vibration on the slope stability and safety is always a challenge for design engineers (Zhou *et al.* 2016).

Ground vibration is indexed by displacement, velocity, and acceleration. Of these, the peak particle velocity (PPV) is used to express blast damages (Faradonbeh *et al.* 2016). This most frequently used parameter is usually calculated using the maximum weight of explosives per delay (Q) and the distance from the charge point (R)

$$PPV = kD^{-b}, \ D = R/Q^{1/2} \tag{1}$$

where PPV is the peak particle velocity (m/s); D is the scaled distance (m/kg$^{1/2}$); k and b are site-specific constants (Kumar *et al.* 2016).

The site-specific constant is calculated based on blast-induced vibration measured on the same site (geological and blast design parameters) (Kuzu 2008, Yilmaz 2016). Kumar *et al.* (2016) summarized 23 various empirical models similar to Eq. (1) from 1959 to 2010. Such as Wei *et al.* (2009), they found that the site-specific constants are not applicable to other sites so that their results cannot be used for other sites. This inconsistency is due to (1) the variable nature of the rock masses which is displayed with k constant; (2) the blast design parameters which is displayed with b constant in empirical models (Taqieddin 1986).

The impact of variability in the rock mass properties during consequences of blasting has been studied. Roy (1991) considered the impact of rock properties and discontinuities in the form of a reducing factor in the propagation of ground vibration and the PPV empirical model (Eq. (1)). Zhu *et al.* (2007) have investigated the effect of joint pacing, joint width, and joint filling material on the fracture patterns using the AUTODYN 2D code. Ma

and An (2008) by use of sample model into the commercial software LS-DYNA argues that discontinuities such as joint planes have strong effect on the blasting-induced rock fractures. Field studies of Hao *et al.* (2001) on joints with angles of 0, 45 and 90° indicated their influence on the attenuation, spectrum and spatial changes of the propagation of the stress wave. Stress wave is produced when the explosive is detonated it pressurizes the blasthole and generates an initial stress that is applied to the rock mass.

Based on statistical analysis in a query mining, Ak and Konuk (2008) found that the frequency of discontinuities in the rock mass is effective in the reduction of seismic wave propagation and applied it as a coefficient in the PPV empirical model. Wang *et al.* (2009) simulated the effect of friction angle and fault dip as two characteristics of discontinuity on the distribution of blast-induced crushed and fractured zones in underground spaces by use of UDEC. Their simulation results showed the significant influence of these two discontinuity features on the rock failure pattern.

Elevli and Arpaz (2010) studied the impact of geological structures and characteristics of explosives and blasting plan by relation diagram method and found the significant impact of these structures. Since the conditions of discontinuities cannot be controlled in the blast results, they proposed to consider the influence of other controllable parameters according to the conditions of discontinuities. Hoek (2012) demonstrated that blasting is the most important factor in the disturbance of rock mass of slopes. Due to changes in the rock mass properties, he proposed the use of numerical models to determine the precise value of disturbance (index "D") in Hoek-Brown failure criterion.

Yan *et al.* (2016) analyzed the role of joints in shaping the profile of blast-induced muck pile with the help of 3DEC. Kekeç *et al.* (2015) experimentally studied the impact of dip, number and the aperture of discontinuities on the propagation of seismic waves in the rock blocks. Based on the results, a graph showed the relation between PPV changes and discontinuity dip. Far and Wang (2016) used a Monte-Carlo sampling for statistical analysis of the impact of some mechanical properties of rocks on the crushed zone radius around the blasthole. According to their results, the changes in mechanical properties of the rock mass are effective in the extension of the radius of crushed zone.

Literature shows the role of various types of geological discontinuities, such as joints, faults, and bedding planes in the propagation and attenuation of dynamic stress waves. But as Kumar *et al.*'s (2016) results showed, previous experimental studies have not considered all field properties and the results of field studies are limited to the same site. The use of numerical modeling as a supplementary tool for other methods provides useful results (Zhuge and Hunt 2003). Accordingly, earlier investigations such as Wang *et al.* (2009) that conducted by two-dimensional numerical modeling provide useful results, but have their own limitations.

Hence, to the above discussion, the aim of this study is to determine the role of fault dip as specific geological discontinuities relative to the direction of the slope face in open pit mines considering peak particle velocity. Due to the advantages of numerical modeling, evaluation was
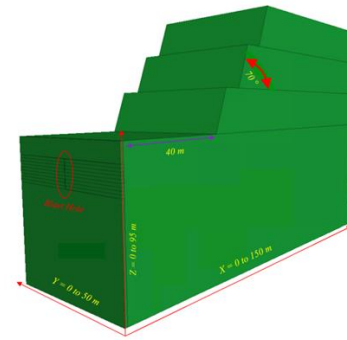

Fig. 1 Configuration of 3DEC model

Table 1 Statistical Properties of the rock material and faults used in 3DEC modeling base on Chadormalu iron ore mine data

Properties (unit)	Value
Density of rock material (ton/m^3)	2.7
Elastic bulk modulus (MPa)	11.1×10^3
Elastic shear modulus (MPa)	7×10^3
Unconfined compressive strength (MPa)	73.7
Unconfined tensile strength (MPa)	7.9
Hoek-Brown parameter, mb	0.894
Hoek-Brown parameter, s	7.9E-5
Discontinuity cohesion (MPa)	4×10^{-2}
Discontinuity friction (Deg.)	30
Normal stiffness of discontinuity (MPa)	60
Shear stiffness of discontinuity (MPa)	30

conducted using three-dimensional discrete element code (3DEC) by monitoring PPVs along a profile. The model includes a slope and three discontinuities and the direction of discontinuities was modeled in different modes. Based on the modeling results, the important issues that should be considered by blast engineers as well as measures to reduce the damages to the slope stability by the dynamic pressure of detonation were proposed.

2. Numerical modelling

In this study, three-dimensional numerical modeling of a slope with three benches with a height of 15 m and a bench slope of 70° was used. The dynamic pressure of detonation was applied on a slope in a hole with a diameter of 200 mm, a charging length of 9 m, and a stemming length of 6 m with the specifications of ammonium nitrate-fuel oil (ANFO) explosives. Fig. 1 shows the details of the developed model.

Given that the effects of discontinuities on the PPVs are concerned, modeling was performed using three-dimensional discrete element code (3DEC). To take account of the effects of discontinuities, three discontinuities with a spacing of 15 m were used.

There are several modes of dip/dip-direction of discontinuities in the slopes of mines, but in this study, four of their ideal modes are considered. Then, the slope is

extended from right to left and the three discontinuities were extended in different modes: (1) discontinuity direction opposite to the direction of the slope face; (2) discontinuity direction along the direction of the slope face; (3) vertical discontinuities; and (4) horizontal discontinuities (Refer to Section 3). The specifications of the slope materials are same as those of diorites in Chadormalu iron ore mine open pit. The physical and mechanical properties of diorites are derived from laboratory test data collected by Kanikavan Shargh Engineering Co. Table 1 summarizes the properties of diorites and discontinuities according to the latest results of laboratory tests on the intact rock samples obtained in the pushback development project of Chadormalu iron ore mine. The properties of the dry samples were used in simulations.

The behavior of the rock mass was modeled using the Hoek-Brown failure criterion. Discontinuities were assumed to show an elastic-perfectly plastic behavior. The Continuously Yielding Joint Model behavioral model can be also used, but given that the most important discontinuities in the slopes have clay fillings without roughness, their tensile strength is significantly reduced after the beginning of displacement and are only under the effect of the cohesion force arising from the weight of the upper rock mass, the elastic-perfectly plastic behavior seems more appropriate.

3. Numerical simulations

Based on Read and Stacey's (2009) suggest on monitor of blast damage, the damage zone can extend at least 95 m above the blasting location. This lead to a 95-meter height for model dimension. Another size of the slope geometry was developed with maximum dimensions of 150×50 m respectively on the axes X and Y based on the four discontinuities modes. Then, the model was solved using the static characteristics of diorite rock in Table 1 to reach initial equilibrium.

Theoretically, the model with a finer mesh size results in a higher accuracy (Wang *et al.* 2006). Kuhlemeyer and Lysmer (1973) showed that for accurate representation of wave transmission through a DEM model, the spatial element size Δl must be smaller than approximately one-tenth to one-eighth of the wavelength λ associated with the highest frequency component of the input wave.

In addition, in order to accurately simulate the transmission of shock waves in rock joints and eliminate the wave distortion, the maximum input frequency of the wave should be less than the computational maximum frequency f_{max}, which is determined by following equations

$$f_{max} = C_s / \lambda \tag{2}$$

$$\lambda = 1/10 \times f_{max} / C_s = 1/10 \times (638/30) \approx 2 \tag{3}$$

where C_s (m/s) is velocity of shear wave (Azizabadi *et al.* 2014).

Therefore, the mesh size of 2 equivalent to one-tenth of

Table 2 Dynamical properties of the rock material and discontinuities used in 3DEC modeling

Properties (unit)	Value
Elastic bulk modulus (MPa)	37.9×10^3
Elastic shear modulus (MPa)	18.5×10^3
Unconfined compressive strength (MPa)	136.7
Unconfined tensile strength (MPa)	47.3

the smallest wavelength was considered. According to Yilmaz and Unlu (2013), the viscous (or absorbing) boundaries were defined on the sides and bottom of the model. This type of boundaries prevents reflection of stress waves into the model. As discussed by Yilmaz and Unlu, a local damping of 5% was considered in this study. Accordingly, if a linear failure criterion is assumed together with the plastic behavior of material, no further damping needs to be assigned as material property. Then, dynamic properties of the rock in Table 2 were inserted and the dynamic pressure of detonation was applied to the model. It should be noted, the bulk and shear modulus is calculated using the Read and Stacey (2009) equations based on statistic properties.

The changes in the dynamic pressure of detonation with time in the blasthole, which is sometimes called wellbore pressure, are divided into two categories of the ideal and non-ideal detonation theories. Ainalis *et al.* (2016) referred to earlier study by Minchinton that non-ideal waves are more accurate to describe the effect of the gas flows, wave interactions, reactive flows and realistic blasthole geometry. ANFO as the most widely used industrial explosive shows non-ideal pressure-time profile (Saharan and Mitri, 2008). To use the accuracy of non-ideal profiles and comprehensive results, the profile of ANFO was used in the modeling.

Due to restrictions on direct measurement of dynamic pressure of detonation within the borehole explosive, pressure-time profile functions are usually used to describe the changes and histories of dynamic pressure. Saharan and Mitri (2008) categorized detonation pressure-time defining functions in (1) Optimized Pressure Profile; (2) Gaussian Function; (3) Pressure Decay; and (4) John-Wilkinson-Lee. In this regard, given the advantages of the pressure decay function defined by Yilmaz and Unlu (2013) study, this type of function was used to develop the profile.

Different pressure decay functions have been defined by various researchers. Duvall (1953) has provided one of the most widely used relations in this regard

$$P_t = P_b(exp(-\alpha t) - exp(-\beta t)) \tag{4}$$

where P_t is pressure-time profile function; α and β are adjustable parameters; and P_b is dynamic pressure of detonation (Pa).

Thereafter, different values were used for the two parameters α and β. For example, Jong *et al.* (2005) developed a relation based on the detonation velocity (V_d) and explosive density (ρ_e). According to the parameters used in this study, the maximum dynamic pressure of detonation equals 1.6 GPa.

$$P_t = 4P_b(exp(-\beta t/\sqrt{2}) - exp(-\sqrt{2}\beta t)) \qquad (5)$$

$$P_b = (\rho_e V_d^2/8)(d_c/d_h)^3 \qquad (6)$$

where β is damping factor (1/s); t is time (s); ρ_e is the density of the unreacted explosive (kg/m³); V_d is the detonation velocity (m/s); d_c/d_h is the ratio of explosive diameter to blasthole diameter (coupling ratio).

In almost identical conditions with input parameters in Eq. (5), Hudson (1993) expressed that ANFO explosive should cause a pressure of 2.6 GPa. Therefore, other pressure decay functions like that provided by Yang *et al.* (2016) were examined. Finally, by using the function provided by Aliabadian and Sharafisafa (2014), a maximum blasthole pressure of 2.5 GPa was obtained. The advantage of Eq. (7) to Eq. (5) is the use of rock density and the propagation of P-waves velocity in the rock. As a result, the pressure decay is also dependent on the rock conditions. Therefore, this equation was used to define the dynamic pressure function (as stress waves). Fig. 2 shows the increase and decrease of pressure versus time.

$$P_t = P_W \frac{8\rho_r C_p}{\rho_r C_p + V_d \rho_e}(exp(-\beta t/\sqrt{2}) - exp(-\sqrt{2}\beta t)) \quad \& \quad \beta = 16338 \quad (7)$$

$$P_W = (P_b/2)(d_c/d_h)^{-qk} \qquad (8)$$

$$P_b = 432 \times 10^{-6} \frac{\rho_e V_d^2}{1+0.8\rho_e} \qquad (9)$$

where ρ_e is the explosive density (gr/cm³); q is shape factor of explosive (2 for cylindrical charges and 3 for spherical charges); k is specific heat coefficient; ρ_r is the rock mass density (gr/cm³); and C_p is the P-wave velocity (m/s).

To apply the dynamic pressure of detonation, Resende (2010) has proposed three methods shown in Fig. 3. In this regard, according to the results recorded by some researchers that the diameter of the hole is effective in the weight of explosives and thereby the blast pressure, loading in the whole blasthole was used. Accordingly, a hole with a diameter of 200 mm was created. To reduce the mesh size, the hole length was divided into 1 m blocks. Using this method, pressure was transmitted more accurately in blast simulations.

Based on the Fish programming language, the codes needed to monitor PPVs were developed along the X-axis and dynamic simulation was performed based on the solution time. The monitoring axes of X=0 to 150 m, Y=25 m and Z=50 m were defined to monitor vibrations created in the working bench of the model.

3.1 Case 1: The discontinuity-free model

Although 3DEC code has been developed for discrete elements, the discontinuity-free model was first simulated to investigate attenuation of the blast pressure. Then, the results were compared with some discontinuities often seen in the slopes. Fig. 4(a) shows the general conditions of the discontinuity-free model. Fig. 4(b) shows PPVs recorded
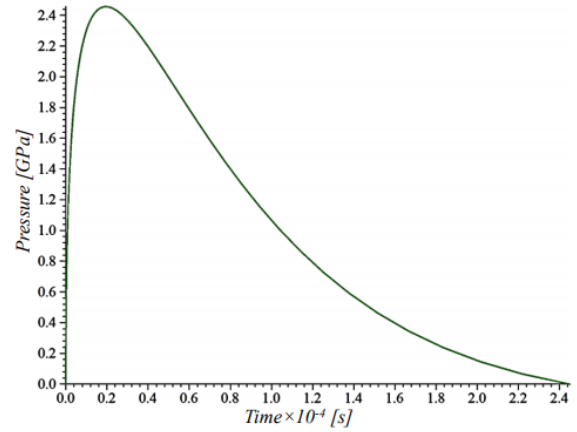

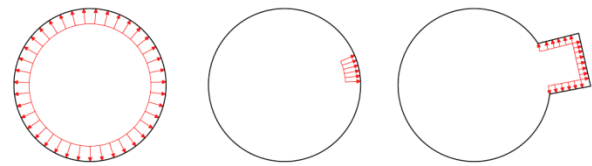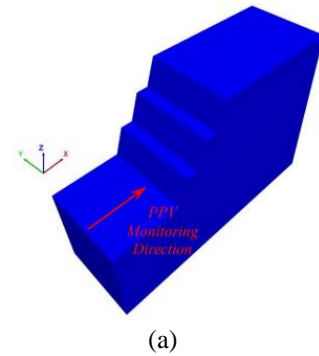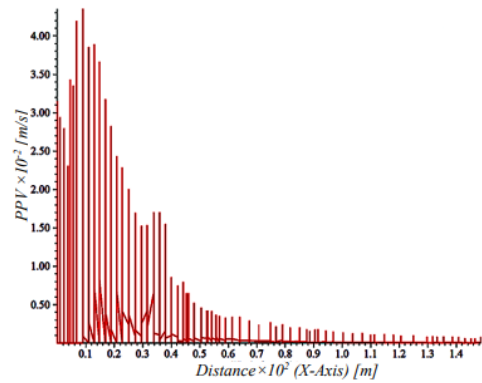Fig. 2 Pressure-Time profile history applying on the blastholes' wall.

Fig. 3 Three methods of the blast load applying, load in the whole blasthole (left), load in an element face (center) and load in the place of a removed element (right)

(a)

(b)

Fig. 4 (a) Discontinuity-free slope model and (b) PPVs recorded along the monitoring axis according to X=0 to 150 m, Y=25 m and Z=50 m

along the monitoring axis.

As can be seen in Fig. 4(b), PPV increases up to a distance of about 10 m after the blasthole. Naturally, the
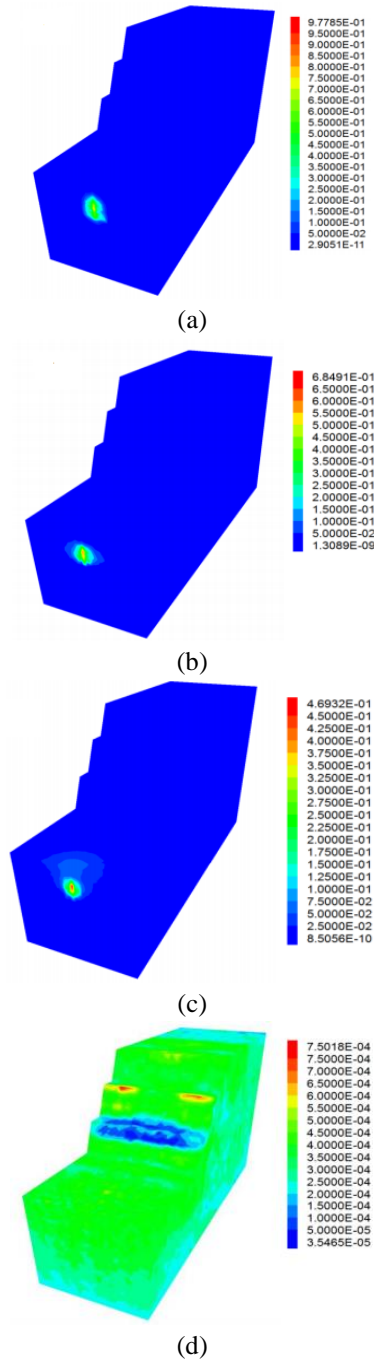
(a)

(b)

(c)

(d)

Fig. 5 Explanation of velocity variation (m/s) in model zones as a function of time after initiation of the explosive in the blasthole. (a) 1 millisecond, (b) 5 millisecond, (c) 0.01 second and (d) 0.1 second

maximum PPV should be recorded at the top of the hole or the zero point. However, (1) given that the diorite stemming is assumed as a 6 m cylinder with free outer boundaries at the blasthole wall. Using this method, it is possible to compress (not displace) stemming due to the dynamic pressure of the explosion and (2) the pressure is transmitted by the meshes to the bench surface, the maximum PPV is recorded at a distance from the hole.

The blast-induced zone predicted by Hustrulid (1999) equivalent to 50-60 times the diameter of the blasthole is
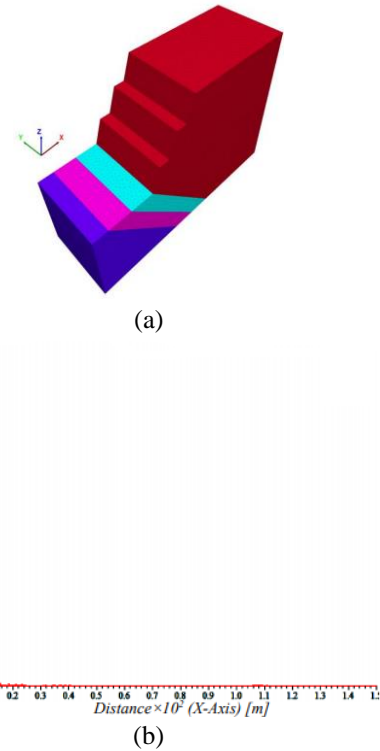

(a)

(b)

Fig. 6 (a) Model configuration with discontinuities opposite to the direction of slope face and (b) PPVs recorded along the monitoring axis

roughly equivalent to a distance of 10 m. Beyond this, the PPV exponentially decreases. Using the recorded values, the relation between PPV and scaled distance was calculated according to Eq. (1) and presented as Eq. (10). This relation has the high coefficient of correlation (R^2). Fig. 5 explains an example of the velocity variation details due to detonation wave in block zones for four states as a function of time after initiation of the explosive.

$$PPV = 0.033 \times (D)^{-1.625}, R^2 = 0.965 \tag{10}$$

3.2 Case 2: Discontinuities opposite to the direction of slope

In this case, the first discontinuity is located at a distance of 10 m from the collar of the blasthole. The distance between the discontinuities is 15 m with a slope of 45° opposite to the direction of the slope face (Fig. 6(a)). As seen in Fig. 6(b), PPV is significantly decreased at a distance of 10 m of the hole due to the incidence of the blast wave with the first discontinuity. PPV remains constant (about a few millimeters per second) up to a distance of 25 m where the second discontinuity is located but due to scale of figures not invisible in Fig 6(b). After incidence to the second discontinuity, PPV reduces to less than 1 mm/s.

3.3 Case 3: Discontinuities along the direction of the slope

In this case, discontinuities are the same as the previous mode, but the direction of discontinuities is the same as the

slope face direction (Fig. 7(a)). PPVs recorded in Fig. 7(b) represent the maximum PPV at a distance of about 10 m from the collar of the hole at the surface of the first discontinuity. Then, the PPV decreases and again increases at the surface of the second discontinuity that is identified at a distance of 25 m from collar. Finally, PPV decline to a few millimeters per second between 25 m to 40 m distance where the second and third discontinuities is identifying.
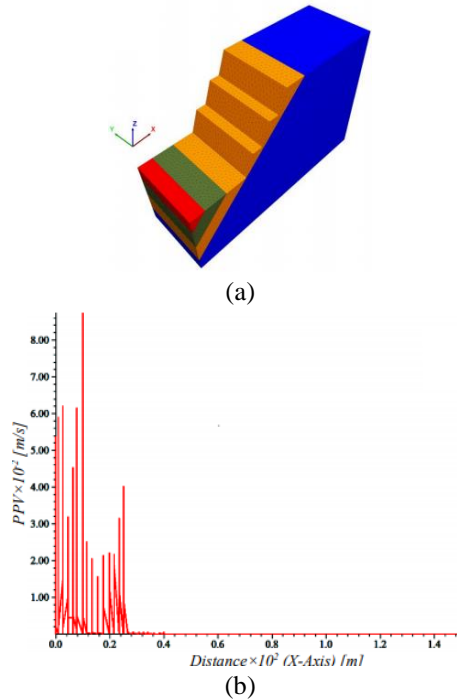

(a)

(b)

Fig. 7 (a) Model configuration with discontinuities along the direction of the slope face and (b) PPVs recorded
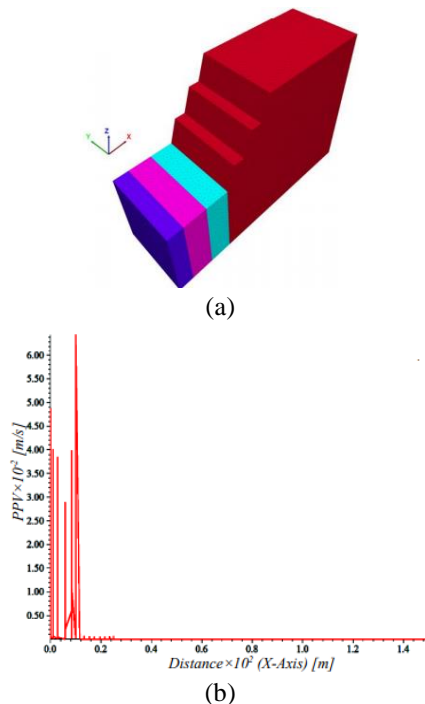

(a)

(b)

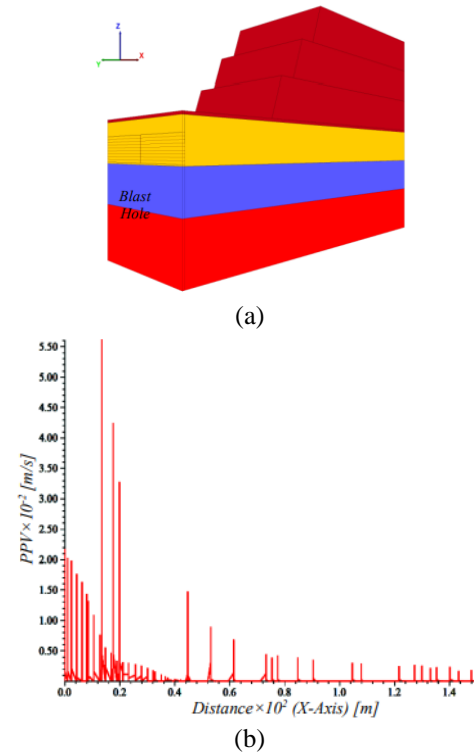Fig. 8 (a) Model configuration with vertical discontinuities and (b) PPVs recorded

(a)

(b)

Fig. 9 (a) Model configuration with horizontal discontinuities; and (b) PPVs recorded

3.4 Case 4: Vertical discontinuities

As shown in Fig. 8(a), three discontinuities with a spacing of 15 m and a dip of 90° have been simulated. The first discontinuity is located at a distance of 10 m from the collar of the hole. According to Fig. 8(b), the maximum PPV is seen at the surface of the first discontinuity and then, PPV instantaneously decreases.

3.5 Case 5: Horizontal discontinuities

Fig. 9(a) shows the last location of discontinuities relative to the slope under study. Fig. 9(b) shows the impact of horizontal discontinuities on PPV. As can be seen, unlike the previous three modes, horizontal discontinuities do not prevent transmission of dynamic pressure, but only lead to a smaller attenuation. So in the presence of horizontal discontinuities in the slope, pressure transmission should be predicted to a large distance of the blasthole.

4. Discussion

As shown in the discontinuity-free model, in the absence of geological discontinuities in the rock, there is an exact relation between PPV caused by dynamic pressure of detonation and the volume of explosives and the distance from the charge point. In other words, PPV empirical models are reliable in rocks lacking discontinuities or tightly jointed rock masses. According to the results of the second to the fifth cases, Eq. (8) cannot be used for the case where the rock mass contains discontinuities with any

direction or dip.

In the case where the direction of discontinuities is opposite to the direction of the slope face, PPV values are limited to the surface of the first discontinuity and due to the discontinuities surface, the stress wave will be reflected in the rock mass. In this case, ground vibration is less propagated leading to less damage to the slope. In the case of same direction of discontinuities and slope, the dynamic pressure of detonation passes through the first and second discontinuities and reaches the third discontinuity with a PPV of a few millimeters per second or even about zero value. In this case, given that the third discontinuity is located at a distance of 40 m from the blasthole, controlled blasting should be used to reduce damages to the slope. For example, a new discontinuity surface can be developed in the rock mass by pre-splitting blasting.

In the case of vertical discontinuities on the working bench, PPV is almost limited to the surface of the first discontinuity as observed in the second case. The difference is that in the second case, PPV decreases from the collar of the hole to the surface of discontinuity, but the maximum PPV is recorded on the surface of discontinuity in this case. Of course, in this case, a part of the stress wave penetrates the surface of the second discontinuity with a PPV value of about a few millimeters per second.

When discontinuities in the rock mass are horizontal, PPV spreads across the model. The maximum PPV is recorded at a distance of 20 m and then, gradually decreases. PPV on the surface of working bench with a low rock mass weight is higher than the bottom of the slopes. In other words, PPV gradually decreases after 40 m where the weight of rock mass in the discontinuities increases.

PPV threshold in Read and Stacey (2009) criteria for damage to hard fresh rock is 375-1000 mm/s. The PPVs recorded in this study are about 0.06 to 0.16 of these criteria (i.e. ~6 cm/s). In other words, there is no damage to the rock mass in this condition and this procedure can be used to predict damages in other geometry and blasting conditions.

Hoek mentioned (1) blast as the most important factor in disturbance of rock mass of slopes and (2) proposed the use of numerical modeling to determine the rock mass disturbance factor. The results showed that numerical modeling can be a good tool for simulating blast and recording PPVs. Comparing the recorded PPVs by the above two criteria, the damage in the rock mass can be indexed and thus the disturbance factor (index D in Hoek-Brown failure criterion) can be determined more accurately.

5. Conclusions

The results of numerical modeling, along with other previous studies, showed that Hoek's suggestion for modeling of disturbance factor estimation of rock masses could provide an ideal technique for realer estimates of D and subsequently the rock mass parameters in Hoek-Brown criterion.

Comparison of PPV graphs obtained from discontinuity-free model against the graphs obtained from other models reflected a huge discrepancy in estimates of PPV and blast-induced damage. Although the coefficient k in the empirical relations represents geological properties, the results showed that geological discontinuities could not be revealed efficiently.

According to the four cases with geological discontinuities scenarios in this study, it is necessary to consider the conditions of discontinuities as a parameter to predict PPV. If direction of discontinuities is opposite to that of the slope face, PPV decreases from its maximum at the top of the collar of hole to the first discontinuity and the minimum ground vibration is transmitted in the rock mass compared to the other three cases. The maximum transmission of the dynamic pressure of detonation occurs when the discontinuities in the rock mass are horizontal. In this case, PPV spreads across the model.

Regarding to their direction relative to the slope face, discontinuities may have beneficial or damaging effects on the transmission and attenuation of the dynamic pressure of detonation. As it could be seen from the perspective of attenuation and dynamic pressure reduction, these discontinuities will have advantageous effects. In order to reduce blast damages, the direction of discontinuities on the surface of working bench should be considered. In this regard, given the advantages of the artificial discontinuities such as those seen in presplitting blast could reduce the destructive effects and rather lead to utilization of positive effects from geological discontinuities.

Comparing PPV values with cracking threshold and damage to the rock mass, the Hoek-Brown criterion disturbance factor can be determined. In this case, the rock mass parameters of this criterion will be closer to reality.

There are different modes of discontinuity dips and direction as well as physical and mechanical properties in open-pit mines. However, attempts were made to examine the four ideal modes of discontinuity for displaying numerical modeling capabilities and completing some of the previous studies.

References

Ainalis, D., Kaufmann, O., Tshibangu, J.P., Verlinden, O. and Kouroussis, G. (2016), "Modelling the source of blasting for the numerical simulation of blast-induced ground vibrations: A review", *Rock Mech. Rock Eng*., **50**(1), 171-193.

Ak, H. and Konuk, A. (2008), "The effect of discontinuity frequency on ground vibrations produced from bench blasting: A case study", *Soil Dyn. Earthq. Eng*., **28**(9), 686-694.

Aksoy, C.O., Uyar, G.G. and Ozcelik, Y. (2016), "Comparison of Hoek-Brown and Mohr-Coulomb failure criterion for deep open coal mine slope stability", *Struct. Eng. Mech*., **60**(5), 809-828.

Aliabadian, Z. and Sharafisafa, M. (2014), "Numerical modeling of presplitting controlled method in continuum rock masses", *Arab. J. Geosci*., **7**(12), 5005-5020.

Azizabadi, H.R.M., Mansouri, H. and Fouché, O. (2014), "Coupling of two methods, waveform superposition and numerical, to model blast vibration effect on slope stability in jointed rock masses", *Comput. Geotech.*, **61**, 42-49.

Duvall, W.I. (1953), "Strain-wave shapes in rock near Explosions", *Geophys.*, **18**(2), 310-323.

Elevli, B. and Arpaz, E. (2010), "Evaluation of parameters affected on the blast induced ground vibration (BIGV) by using relation diagram method (RDM)", *Acta Montanistica Slovaca*, **4**, 261-268.

Far, M.S. and Wang, Y. (2016), "Probabilistic analysis of crushed zone for rock blasting", *Comput. Geotech.*, **80**, 290-300.

Faradonbeh, R.S., Armaghani, D.J., Majid, M.A., Tahir, M.M., Murlidhar, B.R., Monjezi, M. and Wong, H.M. (2016), "Prediction of ground vibration due to quarry blasting based on gene expression programming: a new model for peak particle velocity prediction", *J. Environ. Sci. Technol.*, **13**(6), 1453-1464.

Hao, H., Wua, Y., Ma, G. and Zhou, Y. (2001), "Characteristics of surface ground motions induced by blasts in jointed rock mass", *Soil Dyn. Earthq. Eng.*, **21**(2), 85-98.

Hoek, E. (2012), *Blast Damage Factor*, in *Technical Note for RockNews*.

Hudson. J.A. (1993), *Comprehensive Rock Engineering: Principles, Practice, and Projects*, Pergamon Press, Oxford, U.K.

Hustrulid, W.A. (1999), *Blasting Principles for Open Pit Mining: General Design Concepts*, Balkema, Rotterdam, The Netherlands.

Jong, Y., Lee, C., Jeon, S., Cho, Y.D. and Shim, D.S. (2005), "Numerical modeling of the circular-cut using particle flaw code", *Proceedings of the 31st Annular Conference of Explosives and Blasting Technique*, Orlando, Florida, U.S.A.

Kekeç, B., Gökay, M.K. and Bilim, N. (2015), "Evaluation of the effect of vibrational wave propagation of different artificial discontinuous planes in rock samples", *Arab. J. Geosci.*, **8**(8), 6399-6407.

Kuhlmeyer, R.L. and Lysmer, J. (1973), "Finite element method accuracy for wave propagation problems", *J. Soil Mech. Found. Div.*, **99**(5), 421-427.

Kumar, R., Choudhury, D. and Bhargava, K. (2016), "Determination of blast-induced ground vibration equations for rocks using mechanical and geological properties", *J. Rock Mech. Geotech. Eng.*, **8**(3), 341-349.

Kuzu, C. (2008), "The importance of site-specific characters in prediction models for blast-induced ground vibrations", *Soil Dyn. Earthq. Eng.*, **28**(5), 405-414.

Ma, G.W. and An, X.M. (2008), "Numerical simulation of blasting-induced rock fracture", *J. Rock Mech. Min. Sci.*, **45**(6), 966-975.

Read J. and Stacey P. (2009), *Guidelines for Open Pit Slope Design*, CSIRO Publishing, Melbourne, Australia.

Resende, J.R.P. (2010), "An investigation of stress wave propagation through rock joints and rock masses", Ph.D. Dissertation, University of Porto, Porto, Portugal.

Roy, P.P. (1991), "Prediction and control of ground vibrations due to blasting", *Colliery Gaurd.*, **239**(7), 215-219.

Saharan, M.R. and Mitri, H.S. (2008), "Numerical procedure for dynamic simulation of discrete fractures due to blasting", *Rock Mech. Rock Eng.*, **41**(5), 641-670.

Taqieddin S.A. (1986), "Ground vibration levels: Prediction and parameters", *Min. Sci. Technol.*, **3**(2), 111-115.

Wang, Z.L., Konietzky, H. and Shen, R.F. (2009), "Coupled finite element and discrete element method for underground blast in faulted rock masses", *Soil Dyn. Earthq. Eng.*, **29**(6), 939-945.

Wang, W.H., Li, X.B., Zuo, Y.J., Zhou, Z.L. and Zhang, Y.P. (2006), "3DEC modeling on effect of joints and interlayer on wave propagation", *Trans. Nonferr. Met. Soc. Chin.*, **16**(3), 728-734.

Wei, X.Y., Zhao, Z.Y. and Gu, J. (2009), "Numerical simulations of rock mass damage induced by underground explosion", *J. Rock Mech. Min. Sci.*, **46**(7), 1206-1213.

Yan, P., Zhou, W., Lu, W., Chen, M. and Zhou, C. (2016), "Simulation of bench blasting considering fragmentation size distribution", *J. Impact Eng.*, **90**, 132-145.

Yang, J., Lu W., Jiang, Q., Yao, C., Jiang, S. and Tian, L. (2016), "A study on the vibration frequency of blasting excavation in highly stressed rock masses", *Rock Mech. Rock Eng.*, **49**(7), 2825-2843.

Yilmaz, O. (2016), "The comparison of most widely used ground vibration predictor equations and suggestions for the new attenuation formulas", *Environ. Earth Sci.*, **75**(3), 269.

Yilmaz, O. and Unlu, T. (2013), "Three dimensional numerical rock damage analysis under blasting load", *Tunn. Undergr. Sp. Technol.*, **38**, 266-78.

Zhou, J., Lu, W., Yan, P., Chen, M. and Wang, G. (2016), "Frequency-dependent attenuation of blasting vibration waves", *Rock Mech. Rock Eng.*, **49**(10), 4061-4072.

Zhu, Z.M., Mohanty, B. and Xie, H.P. (2007), "Numerical investigation of blasting-induced crack initiation and propagation in rocks", *J. Rock Mech. Min. Sci.*, **44**(3), 412-424.

Zhuge, Y. and Hunt, S. (2003), "Numerical simulation of masonry shear panels with distinct element approach", *Struct. Eng. Mech.*, **15**(4), 477-493.

CC